ISSN 1063-7834, Physics of the Solid State, 2025, Vol. 67, No. 8, pp. 642–654. © Pleiades Publishing, Ltd., 2025.

Mechanical and Thermal Characterization of Polyoxymethylene: Strain Rate Sensitivity, Crystallinity and Failure Mechanisms

Sid Ahmed Reffas[a,b], M. Elmmaguenni[b], R. Yekhlef[c], D. Belfennache[c], Talal M. Althagafi[d,*], M. Fatmi[e,], and A. Djemli[f,g]**

[a] *Department of Engineering Mechanics, Mohamed Boudiaf University of Oran, Oran, 31000 Algeria*

[b] *Department of Engineering Mechanics, University Djilali Liabes of Sidi Bel Abbes, Sidi Bel Abbes, 22000 Algeria*

[c] *Research Center in Industrial Technologies CRTI, P.O. Box 64, Cheraga, Algiers, 16014 Algeria*

[d] *Department of Physics, College of Sciences, Taif University, P.O. Box 11099, Taif, 21944 Saudi Arabia*

[e] *Research Unit on Emerging Materials (RUEM), University Ferhat Abbas of Setif 1, Setif, 19000 Algeria*

[f] *Faculty of Physics, University of Sciences and Technology Houari Boumediene (U.S.T.H.B), El Alia, BP 32, Bab Ezzouar, Algiers, 16111 Algeria*

[g] *Physics and Chemistry of Materials Lab, Department of Physics, University Mohamed Boudiaf of M'sila, M'sila, 28000 Algeria*

** e-mail: t.althagafi@tu.edu.sa*

*** e-mail: fatmimessaoud@yahoo.fr*

Received March 15, 2025; revised April 29, 2025; accepted May 2, 2025

Abstract—Polyoxymethylene (POM) is a high-performance semi-crystalline thermoplastic widely used for its excellent mechanical strength, wear resistance, and dimensional stability. This study investigates the mechanical and thermal behavior of POM under large deformations through tensile testing and thermal analysis. The results indicate that POM exhibits linear elastic behavior at low strains, transitioning to nonlinear viscoelastic and plastic behavior at higher deformations. Stress whitening and microvoid formation significantly influence failure mechanisms. Differential Scanning Calorimetry (DSC) and Thermogravimetric Analysis (TGA) confirm POM's high crystallinity (~40%) and thermal stability, with a melting temperature of 166°C. Scanning Electron Microscopy (SEM) reveals cavitation and fibrillation as dominant damage mechanisms. The findings highlight the challenges of substituting POM due to its unique property balance. Further research should focus on predictive plasticity models to optimize POM's industrial applications.

Keywords: polyoxymethylene (POM), mechanical properties, thermal analysis, strain rate sensitivity, microstructural analysis, large deformation

DOI: 10.1134/S1063783425601560

1. INTRODUCTION

Research on the evolution of morphology in the field of polymer science and technology is of great importance, as it impacts the final characteristics of many polymer materials [1, 2]. Polymer blends are often separated as a temperature [3, 4]. Polymer degradation kinetics have been studied across different materials and conditions [5]. Lua and Su [6] examined polyimide pyrolysis using Kissinger methods, while Morancho et al. [7] compared thermoset coatings. Mamleev et al. [8] developed model-free methods for activation energy calculation. Semi-crystalline polymers, such as polyacetal (POM), are used in various industrial applications due to their excellent mechanical, thermal, and chemical properties. However, setting up and conducting mechanical tests on these materials requires a rigorous approach to capture the different aspects of their behaviour under various loading conditions. For example, tensile tests conducted on POM must consider assumptions of homogeneous or isochoric deformation and transverse isotropic deformation to accurately describe the material's mechanical properties [9]. POM is valued for its rigidity, wear resistance, and good tribological properties. Under low deformations, POM behaves as a linear elastic material under static loads and as a linear viscoelastic material under vibratory loads. For larger deformations, POM exhibits nonlinear viscoelastic behaviour and can even behave as a plastic or viscoplastic material. These characteristics have been extensively studied in recent years, with particular attention to the deformation mechanisms at the molecular scale and their effects at the macroscopic scale.

Polyoxymethylene (POM) is a highly crystalline thermoplastic distinguished by its exceptional strength

and rigidity, complemented by excellent sliding properties, wear resistance, and minimal moisture absorption. These characteristics, along with its outstanding dimensional stability, fatigue resistance, and chemical resilience, establish POM as a versatile construction material suitable for diverse applications, particularly in the production of intricate, small components requiring superior surface quality [10–12]. While the incorporation of fillers organic, mineral, glass, and others can further enhance its strength, rigidity, and dimensional stability, it's worth noting that such modifications may potentially compromise certain other properties of the material.

There are a multitude of thermal analysis techniques for polymers, whose information is complementary and enables the precise identification of the properties and transitions of materials, as well as their evolution.

The implementation of mechanical tests on flat POM specimens is a crucial part of this work. These tests are conducted at ambient temperature and are designed to evaluate the influence of the type of control (e.g., displacement control or force control) and the measurement principle (assuming homogeneous/isochoric deformation versus transverse isotropic deformation) on the material's response [13, 14]. A precise understanding of these aspects is essential to provide a comprehensive description of the mechanical properties of POM and to elucidate the mechanisms of deformation, damage, and fracture. Mechanical testing of semi-crystalline polymers, such as POM, often encounters challenges due to the amorphous nature of some materials and the inherent variations in additive manufacturing techniques [15, 16], such as Fused Deposition Modeling (FDM).These challenges can lead to uneven distribution of failure cases among the tested specimens, necessitating a larger number of standardized specimens to obtain accurate results. Consequently, it is recommended to test an additional sample per batch beyond the number prescribed by specific standards. The results of these tests play a crucial role in understanding and characterizing the mechanical properties of POM under large deformations. The main objective of this study is to provide a detailed description of the mechanical properties of POM under large deformations to better understand the mechanisms of deformation, damage, and fracture of this material. This in-depth understanding will contribute to the optimization of industrial applications of POM and the improvement of processing and shaping methods. In the literature, many authors mention that PET initially whitens in the amorphous phase during its plastic deformation in tension [17–19]. The variation in the material's birefringence is caused by the formation of microvoids within the material. These microvoids organize in such a way as to create cracks that propagate perpendicularly to the direction of the mechanical force [20–24]. In the past, initiation methods have sparked debates. A synthesis of the main mechanisms was conducted by Bucknall [25]. It is evident that the preferred initiation sites are the interchain shear zones, which, when restricted by the matrix entanglements, lead to the appearance of this volumetric damage [26, 27]. It is therefore essential to take into consideration the impact in the calculation of the actual mechanical stress endured by the material [28–30]. Thus, by identifying intrinsic behavioural laws, it is possible to interpret the impact of the actual strain rate and temperature.

This study investigates the mechanical and thermal behaviour of polyoxymethylene (POM) under large deformations, focusing on fracture mechanics, stress triaxiality, and failure mechanisms to enhance its industrial performance. As the manuscript concludes, no single material can match all of POM's advantageous characteristics, with each alternative presenting trade-offs in mechanical performance, thermal resistance, or processing properties. The development of suitable replacements requires sophisticated plasticity models incorporating damage mechanisms like void growth and coalescence, necessitating application-specific compromises rather than universal solutions. The findings are crucial for optimizing POM in automotive, aerospace, and medical applications, where its high strength, wear resistance, and thermal stability make it ideal for lightweight structural components, precision mechanical parts, and biomedical devices operating under demanding conditions.

2. EXPERIMENTAL SECTION

2.1. Materials

The material examined in this study is a polymer known as POM (polyacetal), in accordance with ISO standards. It is available in two variants: copolymer (POMC) and homopolymer (POMH), which have slight differences. POM is a semi-crystalline, opaque polymer that is naturally white but is commonly produced in various colors. It has a molar mass of 10 kg/mol, a density of 1200 kg/m^3, and a specific gravity ranging from 1.41 to 1.42 g/cm^3.

According to analyses by differential scanning calorimetry at a constant heating rate of 10°C/min, the extruded material exhibits a glass transition temperature of 75°C, a melting temperature of 166°C, and a cold crystallization temperature of 145°C. The crystallinity of the extruded sheets is zero since, during the initial heating, the enthalpies of cold crystallization and melting are identical (Fig. 1).

2.2. Experimental Technique

Understanding the mechanisms of deformation and damage requires exploring the mechanical response of the material under different conditions. As with other classes of materials, the mechanical

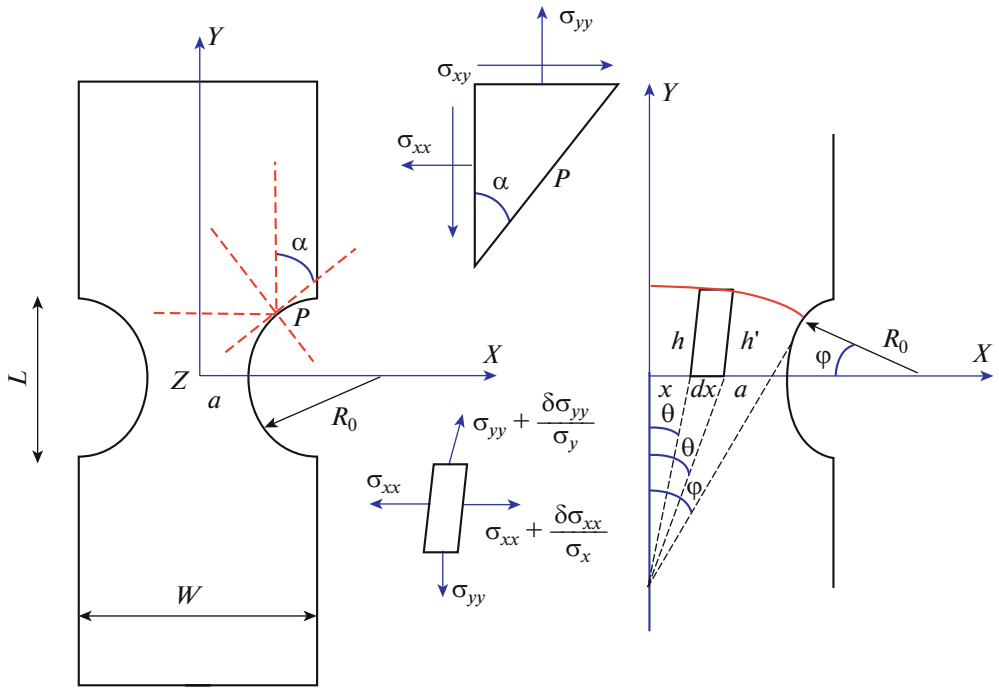

Fig. 1. Schematic for constraints analysis.

response of POM depends on the type of test, the loading conditions, and the geometry of the specimens used. Mechanical tests aim to characterize the material behaviour laws. A behaviour law establishes a relationship between stresses and strains. Based on Bridgman's analysis of the stress state during necking in a uniaxial tensile bar later expanded upon by Hill [31] a flat specimen is considered for evaluation. The proposed hypothesis assumes that deformation within the specimen's minimum cross-section is uniform. This assumption holds reasonably well for specimens with slight notching. However, the presence of a notch introduces additional stress components that deviate from the uniaxial loading direction. Currently, no exact analytical solution exists to describe the complete stress and strain fields in a notched specimen. To accurately characterize the stress distribution under plane stress conditions, particularly near the notch, a schematic of the specimen geometry is shown in Fig. 1a, accompanied by a detailed diagram of the stress distribution in Fig. 1b.

To analyze the tests on the evolution of the behaviour of our polymer under a state of plane stress, we have considered the behaviour of our material to be assumed to be perfectly elastic–plastic. This assumption is invalid for most polymer materials due to their large deformations. However, obtaining equilibrium equations for large deformations is very complex. In a Cartesian coordinate system, the mechanical equilibrium is then expressed as:

$$\sigma_{ij} = 0, \tag{1}$$

when using flat test tubes with thin thicknesses, we assume that the stress distribution is planar, meaning that the stress representing the normal direction to the surface is considered zero and that the radial displacement in the minimum section is, therefore, proportional to the width. It is also inferred that the radial and circumferential deformations are equal and constant. Thus, the stress and strain tensors take the following form:

$$\sigma = \begin{pmatrix} \sigma_{xx} & \sigma_{xy} & 0 \\ \sigma_{yx} & \sigma_{yy} & 0 \\ 0 & 0 & 0 \end{pmatrix} \tag{2}$$

and

$$\varepsilon = \begin{pmatrix} \varepsilon_{xx} & \varepsilon_{xy} & 0 \\ \varepsilon_{yx} & \varepsilon_{yy} & 0 \\ 0 & 0 & \varepsilon_{zz} \end{pmatrix}. \tag{3}$$

This yields the following equilibrium equations:

$$\begin{cases} \sigma_{xz} = \sigma_{yz} = 0 \\ \dfrac{\partial}{\partial z}[\ ] = 0 \\ \sigma_{zz} = 0. \end{cases} \tag{4}$$

Therefore, any point at the end of the notch depends only on two directions (x and y):

$$\begin{cases} \sigma_{xx}\cos\alpha = \sigma_{xy}\sin\alpha \\ \sigma_{yx}\cos\alpha = \sigma_{yy}\sin\alpha. \end{cases} \tag{5}$$

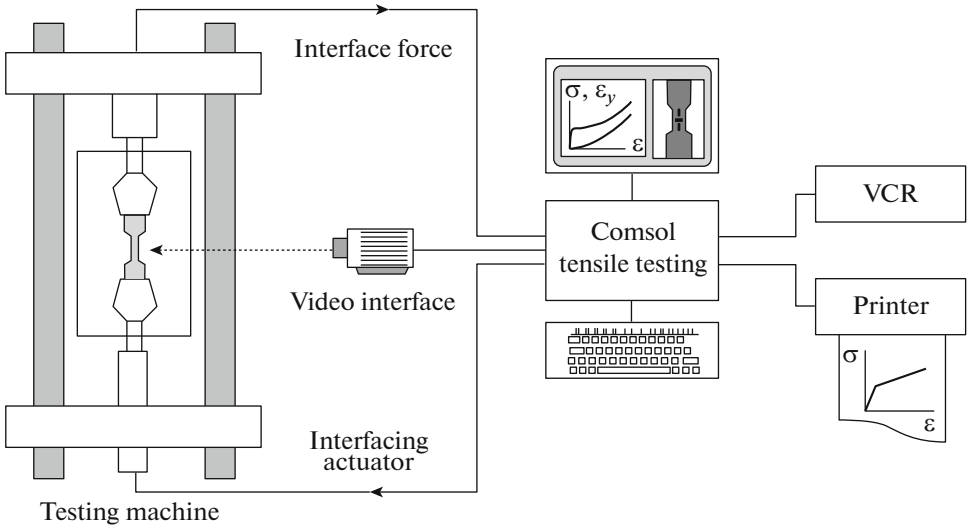

Fig. 2. INSTRON 5867 press (tensile setup).

In this case, the equations will be written as follows:

$$\begin{cases} \sigma_{xx} = \sigma_{yy} \tan^2 \alpha \\ \sigma_{yx} = \sigma_{yy} \tan \alpha. \end{cases} \quad (6)$$

At the notch center $Y = 0$, where $a = 0$, we obtain:

$$\begin{cases} \sigma_{xx}\big|_{x=0} = 0 \\ \sigma_{yx}\big|_{y=0} = 0, \end{cases} \quad (7)$$

$$\left.\frac{\partial \sigma_{yy}}{\partial y}\right|_{y=0} = 0. \quad (8)$$

The deformation along the Z-axis is given by the following formula:

$$\varepsilon_{zz} = -\frac{1}{2}(\varepsilon_{xx} + \varepsilon_{yy}). \quad (9)$$

However, under these conditions of plane constraints, we assume that the constriction occurs after plasticization, and the equivalent stress used is given by the following formula:

$$\sigma_{eq} = \sqrt{\frac{1}{2}\left[(\sigma_{xx} - \sigma_{yy})^2 + (\sigma_{yy} - \sigma_{zz})^2 + (\sigma_{zz} - \sigma_{xx})^2\right]}. \quad (10)$$

Based on these analyses, we can obtain straightforward solutions if the following conditions are met:

$$\sigma_{yy} = \sigma_{xx} + \sigma_{yy}\big|_{y=a} = \sigma_{xx} + F, \quad (11)$$

or $F = \sigma_{yy}\big|_{y=a}$.

The constraint in the Y direction satisfies the Von-Mises plasticity condition. This is a simplified equation where the longitudinal effort is considered uniform across the entire section. However, it is possible to find another solution to solve the constraint equation in the transverse part of the constriction by assuming that the contour forms a closed surface in the notch (Fig. 1b).

Based on Eq. (4), the main constraint line is perpendicular to the notch axis and the center axis of the specimen. It is reasonable to approximate by bringing the main constraints closer through a circle, with its center located on the central axis (Fig. 3a).

Through a line perpendicular to the x-axis passing through point x, other lines can be constructed for the main constraints, assuming that these lines also form a circle, and that the notch circle of the test specimen is also constructed by these lines. For a very small angle f, the notch radius is considered R, and the circle radius is R', where $R' = a/\varphi$.

For a small section element with a unit width in the z direction, bounded by x and $x + dx$, corresponding to the angle between the two axial lines θ and θ', the following equations can be obtained:

$$\begin{cases} \theta = \dfrac{x\phi}{a} \\ \theta' = \dfrac{(x + dx)\phi}{a} = \dfrac{x\phi}{a} + \dfrac{dx\phi}{a}. \end{cases} \quad (12)$$

Balancing efforts in the x direction yields the following relationship:

$$\left(\sigma_{yy} + \frac{\partial \sigma_{yy}}{\partial_y} dy\right) \sin\theta\, dx - \sigma_{xx} h + \left(\sigma_{xx} + \frac{\partial \sigma_{xx}}{\partial x} dx\right) h' = 0. \quad (13)$$

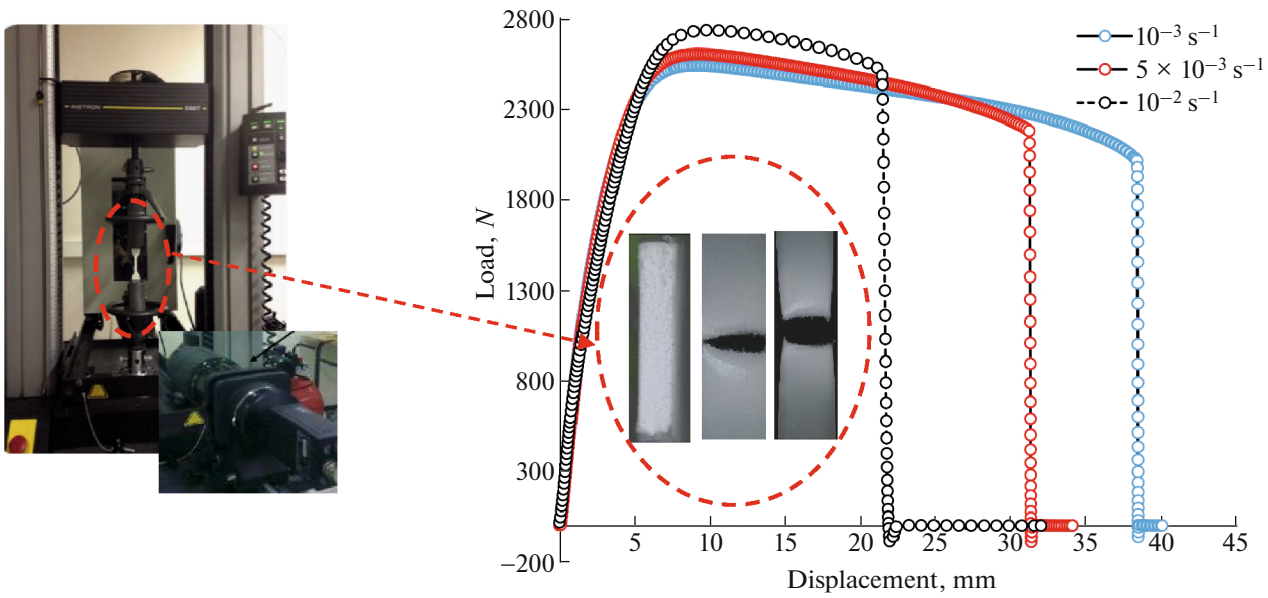

Fig. 3. True stress-true strain under different strain rates.

Based on the geometry of a flat specimen, the following relationship is obtained:

$$\begin{cases} h = R\phi + R'(\cos\theta - \cos\phi) \\ h' = R\phi + R'(\cos\theta' - \cos\phi). \end{cases} \quad (14)$$

By substituting Eq. (12) into Eq. (14), with a small value of φ, and by introducing the following formula $\cos x = 1 - (x^2/2)$; we obtain the following equations:

$$\begin{cases} h = \phi\left(R + \dfrac{a^2 - x^2}{2a}\right) \\ h' = \phi\left(R + \dfrac{a^2 - x^2}{2a} - \dfrac{x}{a}dx\right). \end{cases} \quad (15)$$

By substituting Eq. (15) into Eq. (13) with $\sin x = x$, we obtain the following equations:

$$\frac{d\sigma_{xx}}{dx} = -\frac{Fx}{a\left(R + \dfrac{a^2 - x^2}{2a}\right)}. \quad (16)$$

By integrating Eq. (16) into Eqs. (17) and (8), we ultimately obtain an approximate solution for the stress component σ_{xx}

$$\sigma_{xx} = F\ln\left(\frac{a^2 + 2aR - x^2}{2aR}\right). \quad (17)$$

By adding Eq. (17) to Eq. (11) with the same boundary conditions as previously used, we ultimately obtain solutions for the other stress components

$$\begin{cases} \sigma_{yy} = F\ln\left(1 + \ln\left(\dfrac{a^2 + 2aR - x^2}{2aR}\right)\right) \\ \sigma_{zz} = 0. \end{cases} \quad (18)$$

For a flat specimen with a groove of radius *Rx* at the bottom of a notch, leaving a remaining neck in the minimum section, the calculation of stress and strain distributions is very complex and cannot be fully resolved analytically. A tensile test involves subjecting a standardized specimen to a tensile force, typically until failure. Unless otherwise specified, the test is conducted at room temperature (20°C). The strain measurement system relies on the use of a CCD video camera interfaced with a PC and mounted on a motorized stand, along with software enabling real-time image processing (Fig. 2). Video measurement allows for obtaining the deformations of materials under stress. It effectively replaces the use of mechanical extensometers in the vast majority of cases, particularly for large deformations and special environments. Its versatility enables adaptation to various specimen sizes and deformation paths. It directly provides stress-strain data for materials at imposed true strain rates. The method also allows for imposing a constant true radial strain rate and real-time measurement of the evolution of true axial stress. However, this measurement technique allows for a more rational analysis of complex and varied experimental data.

The specimen, with a precisely defined geometry having average dimensions of 110 × 10 × 4 mm, is clamped at both ends into jaws or grips. One of these grips, fixed, is connected to a dynamometric system for force measurement by means of a ball joint so that the axis of the applied forces coincides with that of the specimen; the other grip, movable, is connected to a drive system at constant speed of displacement, or more rarely, constant load. Dynamometric determinations (force measurements) are conducted using electronic sensors, typically consisting of a highly rigid

elastic element (beam, ring, etc.), whose slight deformation due to the applied force is measured using an electrical system (strain gauges, variable inductances, capacitances, ...).

In the case of a flat specimen (under plane stress), the local true axial strain and stress are given by the following relationships:

$$\sigma_{yy} = \frac{F}{(S_0/\exp(\varepsilon_{zz}))}. \quad (19)$$

3. RESULTS AND DISCUSSION

The mechanical tests aim to characterize the material behaviour laws. A behaviour law establishes a relationship between stresses and strains. The tests are conducted at controlled strain rates and at a temperature of 20°C. Large deformation tests were performed on an electromechanical machine of the Instron type (model 5867).

In Fig. 3, it can be observed that for deformations in the range of 3–5%, the higher the strain rate, the higher the stress at the plastic yield point σ_0. Beyond this point, there is noticeable softening, followed by a long plateau that ends with the onset of hardening. The Young's modulus is determined in the linear part of the stress-strain curve, and the end of this linear part represents the elastic limit, which occurs before the stress peak σ_y. Tensile tests at different strain rates provide information about the nature of polymers.

The yield stress and strain were determined graphically between the perfectly elastic region and the onset of plasticity of the true stress-strain curve (Fig. 4). We thus see that when the deformation speed decreases, the initial plastic plateau is increasingly longer, the hardening stage being delayed. The threshold stresses a was determined graphically between the perfectly elastic domain and the beginning of plasticity of the true stress—true strain curve.

The mechanical properties of the polyacetal for the different speeds are given in Table 1.

The intersection of the origin tangent and the plateau tangent provides a value for the mechanical parameters. Therefore, we propose to adopt this latter definition to determine the threshold plastic stress for all triaxialities. This evolution, as shown in Fig. 5, illustrates the dependence of POM threshold behavior on strain rate. In a first approximation, this evolution can be correlated by a linear regression with a relatively low slope. Figure 6 presents data on the variation of Yuong modulus and POM energy on different samples. The graph shows two sets of data: one for Young's modulus (a measure of stiffness of a material) in percentage terms (E%), and another for energy in joules (J). A black dotted line with data points indicates the trend in energy values, with error bars suggesting variability or uncertainty in the measurements. Similarly, Young's modulus also has error bars, although no connecting lines are drawn between these points. From the data, it appears that the Young's modulus peaks at sample 2 and then decreases, while the measured energy shows a less clear trend but appears to decrease slightly after sample 2.This figure could suggest a correlation between Young's modulus and the energy characteristic of a new material or coating design, possibly indicating optimal properties for sample 2. The innovation may lie in how these two properties interact or are optimized in the new material design. This could imply that the stiffness of the material (Young's modulus) has a direct effect on its energy absorption or release characteristics (POM energy), which is important for applications where mechanical stiffness and energy management energy are crucial.

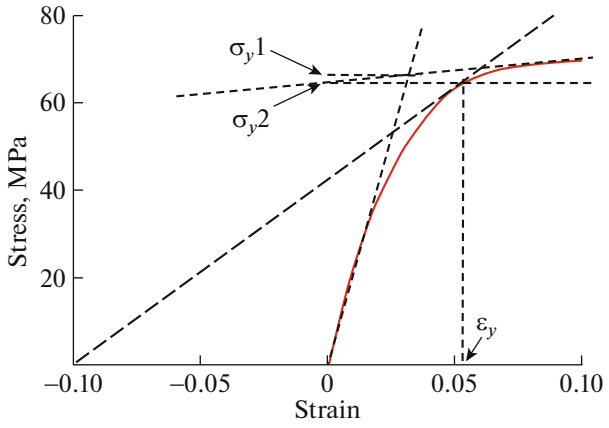

Fig. 4. Explanations of the plastic threshold.

Figure 7 shows a comparative analysis of impact strength and energy on five different samples, presumably of one material, given the abbreviation POM that is commonly used for this thermoplastic. On the chart there are two sets of data. A bar represents the impact resistance in kilojoules per square meter (R_e (kJ/m^2)), corresponding to the main y-axis on the left, and the other mean energy in joules (energy (J)), which relates to the secondary y-axis on the right.

The variability or precision of measurements. Likewise, a dotted line connects the data points above the orange bars, again with error bars. From the graph, we can observe that the impact strength shows a pronounced peak at sample 2 and then decreases. The energy also peaks at sample 2 but experiences a less

Table 1. Mechanical properties of polyacetal

$d\varepsilon/dt$, S^{-1}	E, MPa	σ_y, MPa	ν
0.0001	2143	63	...
0.0005	2254	66	0.38
0.001	2325	70	....

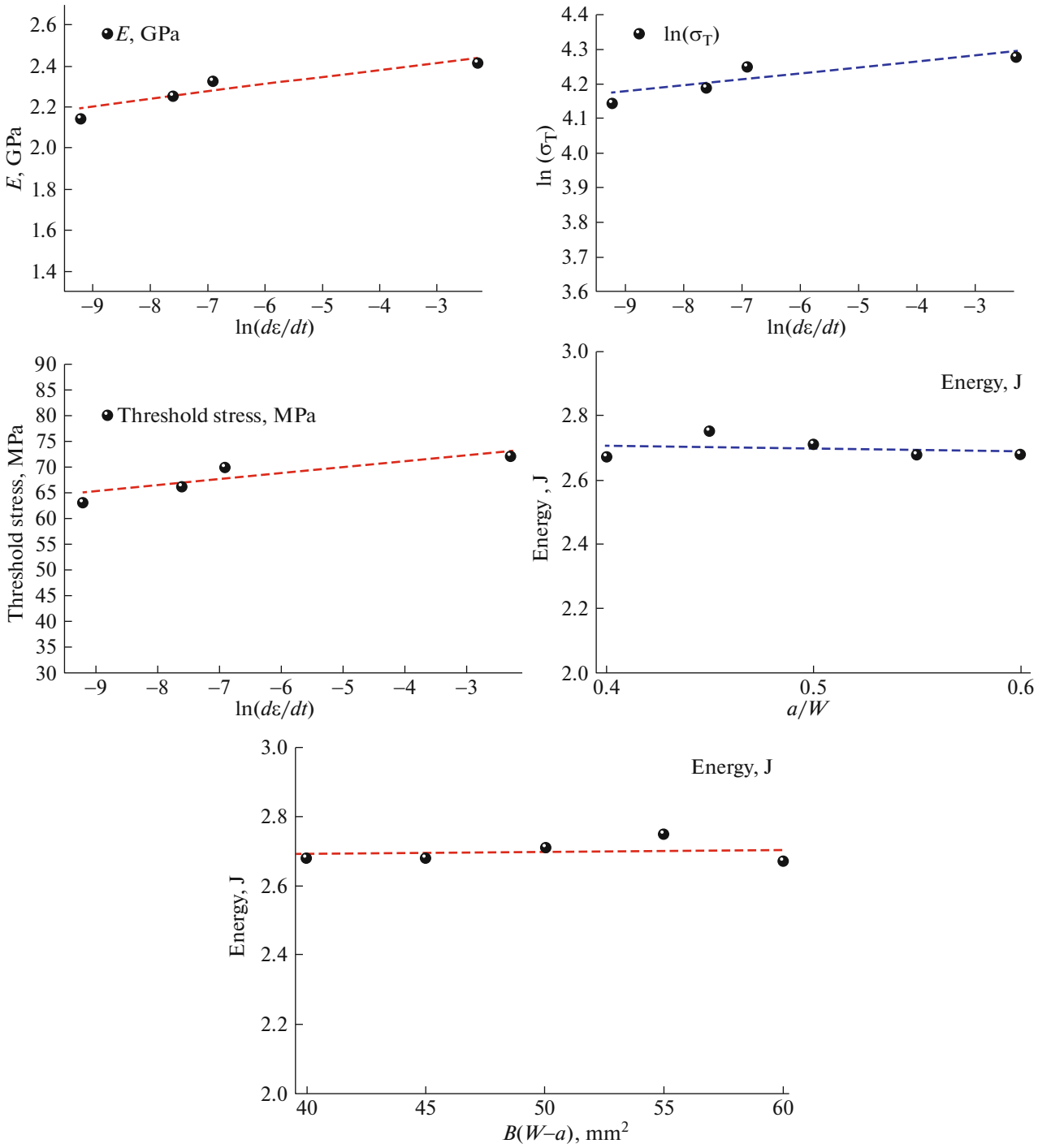

Fig. 5. Dependence of mechanical parameters on deformation rate.

dramatic drop. There is a clear correlation between the trends in both properties, with sample 2 representing a peak in both impact resistance and energy. This figure can be used to illustrate the mechanical properties of a new POM coating design. The focus would likely be on how the material's impact resistance correlates with its energy characteristics, which could be crucial for applications requiring materials that not only effectively absorb shock, but also effectively retain or dissipate impact. energy. Innovation may lie in the formulation or processing of POM to improve these properties, with sample 2 possibly representing an optimized balance between impact resistance and energy management. Such a balance could be critical

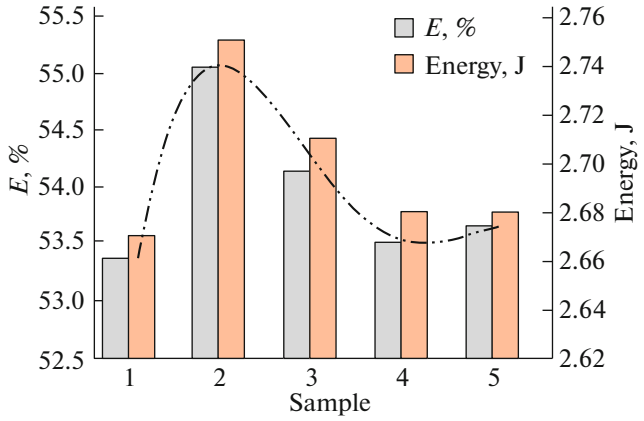

Fig. 6. Dependence of young modulus and POM energy of polyoxymethylene (POM).

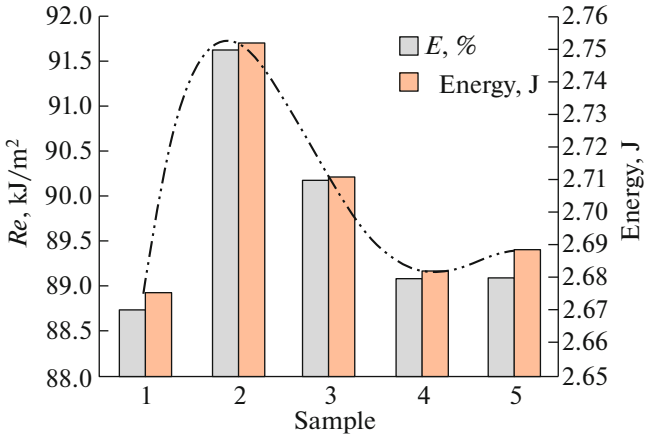

Fig. 7. Dependence of impact strength and energy of polyoxymethylene (POM).

to the material's function and purpose in practical applications, such as automotive parts, consumer electronics, or mechanical gears, where durability and impact resistance are essential.

Figure 8 presents micrographs of the fracture surface, confirming the presence of voids. Additionally, damage bands composed of numerous aligned and elongated voids are observed, with an average size of approximately 500 nm. A comparison of the images reveals that the deformation mechanisms are significantly affected by stress triaxiality: at high triaxiality levels, pronounced cavitation and fibrillation occur, while at lower triaxiality, only a few scattered voids are present.

Figure 9 shows the variation of stress as a function of strain and a comparison of the monotonic response of POM in uniaxial tension at a strain rate of 10^{-1} s^1. This figure highlights the influence of the loading path on the behaviour law of POM. The behaviour exhibits nearly zero hardening with a progressive stress drop after a strain greater than 5.5%.

During the presentation of the thermogravimetric analysis of POM (Fig. 10), it was explained that this method is used to characterize the physical and chemical properties of materials as a function of temperature in a precisely controlled atmosphere. A significant peak is observed around 30 min, corresponding to the period of rapid weight loss. This indicates that the decomposition or volatilization of the material is maximal at this temperature. The graph indicates a thermal reaction or decomposition of a material, with a critical temperature around 310°C, where the weight loss is most significant. This is visualized by the rapid drop in weight and the peak in the weight derivative.

The technique used to evaluate the crystallinity ratio x_c of POM is differential scanning calorimetry (DSC) at a heating rate of 10°C/min under nitrogen. The apparatus used is a Perkin-Elmer DSC Diamond.

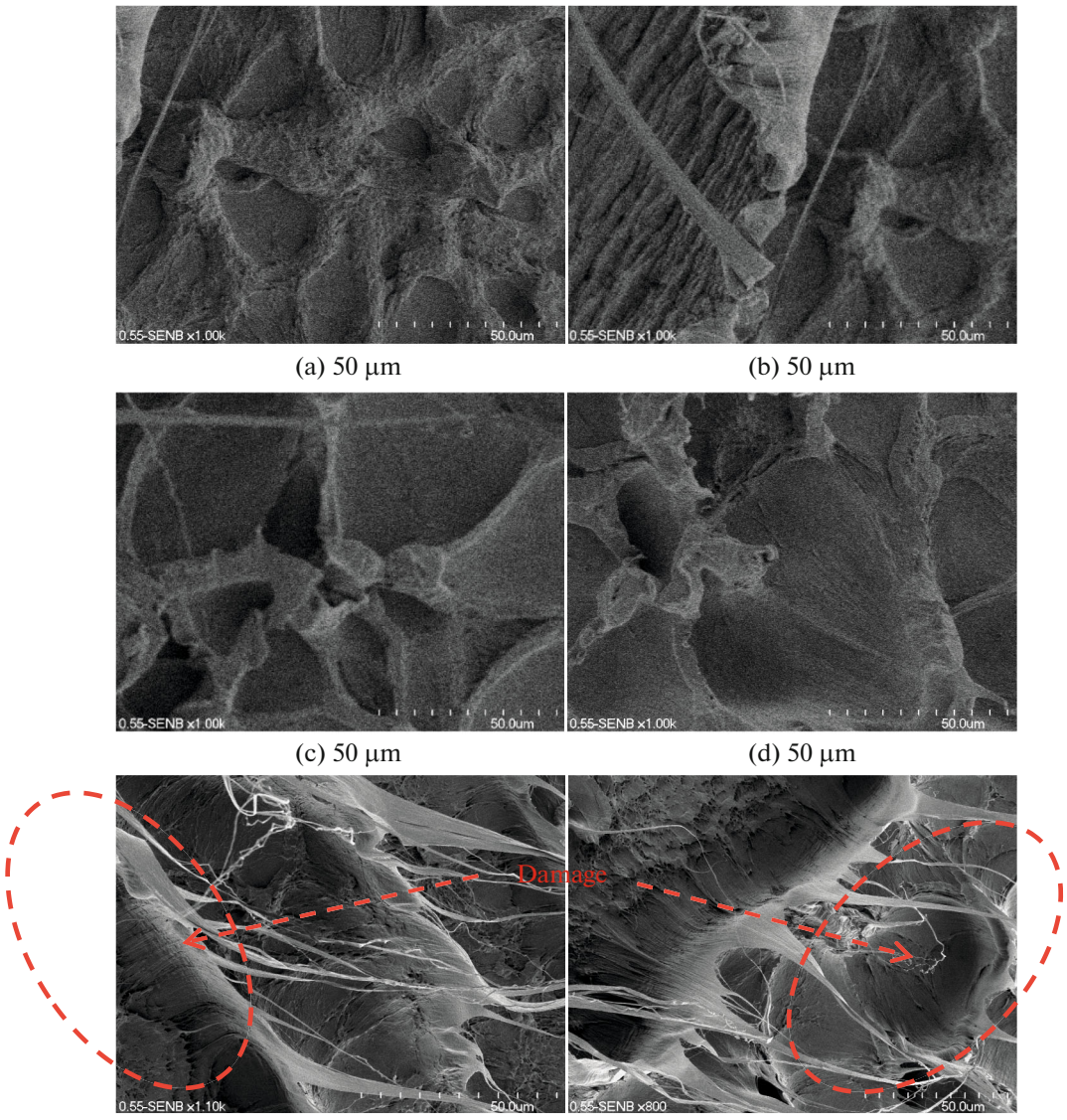

Fig. 8. Observations (MEB) of the fracture surface: (a–d) positions surrounding the initiation zone, (e) and (f) initiation zone of polyoxymethylene (POM).

The crystallinity ratio x_c is determined using the following relationship:

$$x_c\ (\%) = \frac{\Delta H}{\Delta H_0} \times 100, \qquad (20)$$

where ΔH is the measured fusion enthalpy and ΔH_0 is the theoretical fusion enthalpy of purely crystalline POM. The melting point T_m was also determined using the DSC technique. This temperature corresponds to the maximum value of the peak. The thermographs corresponding to the three positions are shown in Fig. 11. The crystallinity ratio of POM is around 40%.

During the DSC analysis presentation, we saw that this method is capable of providing us with values such as the melting temperature, the crystallization temperature, and the crystallization rate. The DMA analysis allowed us to obtain the following values: the storage modulus in tension E', the corresponding loss modulus E'', and the mechanical loss angle tanδ.

Figure 12 shows curves representing two quantities: the storage E' and the loss modulus E'' as a function of temperature. At low temperatures, the storage modulus (E') is high, which means that the material is rigid and retains elastic energy well. As the temperature increases, the storage modulus (E') decreases, while the loss modulus (E'') increases, indicating a transition in the material's behaviour, possibly from a glassy

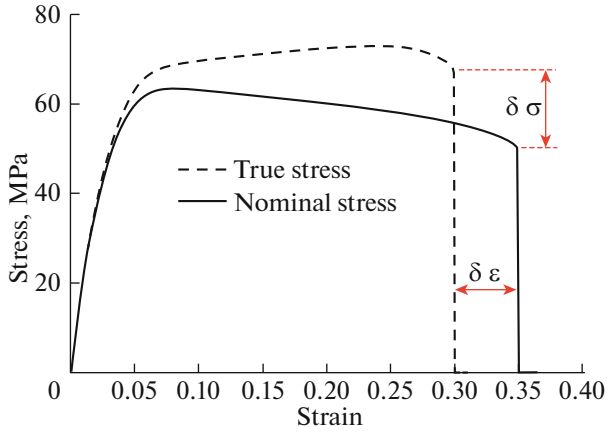

Fig. 9. Dependence of stress as a function of strain of polyoxymethylene (POM): comparison between nominal and the true curve.

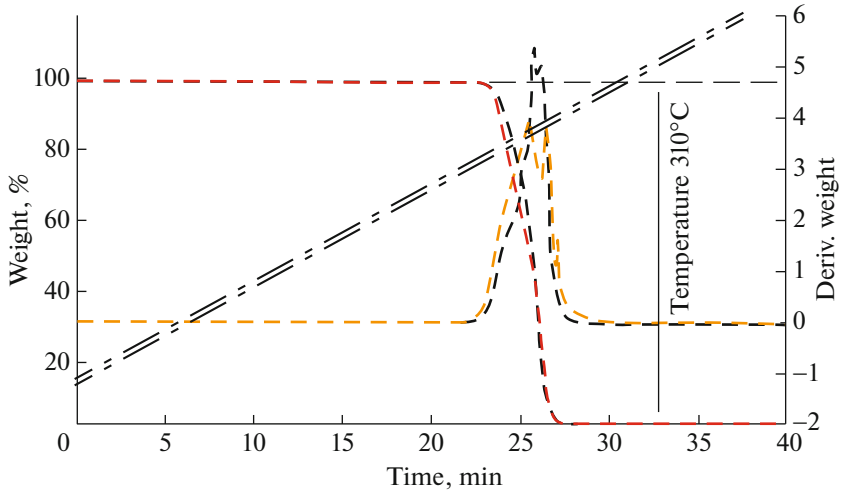

Fig. 10. Isothermal thermograms of polyoxymethylene (POM) at 310°C.

state to a rubbery state. The peak of the loss modulus (E'') could indicate a glass transition temperature (T_g), at which the material begins to lose its rigidity and becomes more viscous.

The tanδ curve also shows a peak at this temperature, confirming a significant transition in the material's structure. The graph represents a typical glass transition behaviour, where a material transitions from a rigid state to a more flexible state as the temperature increases.

4. CONCLUSIONS

As anticipated from the outset, substituting Polyoxymethylene (POM) will not be an easy task. Given its specific and unique properties, finding an equivalent material poses significant challenges. POM is known for its high strength, rigidity, low friction, excellent wear resistance, and stability under varying environmental conditions. These attributes make it an ideal material for a wide range of applications, particularly in the automotive, consumer electronics, and industrial sectors. Despite the identification of potential substitutes, it is evident that no single material can match all the advantageous properties of POM. Each alternative comes with its own set of trade-offs, whether it be in terms of mechanical performance, thermal resistance, or processing characteristics. Therefore, the selection of a substitute will likely depend on the specific requirements of the application, with compromises being made on certain properties. To further model and predict the behaviour of materials that could replace POM, it will be necessary to develop a sophisticated plasticity model that incor-

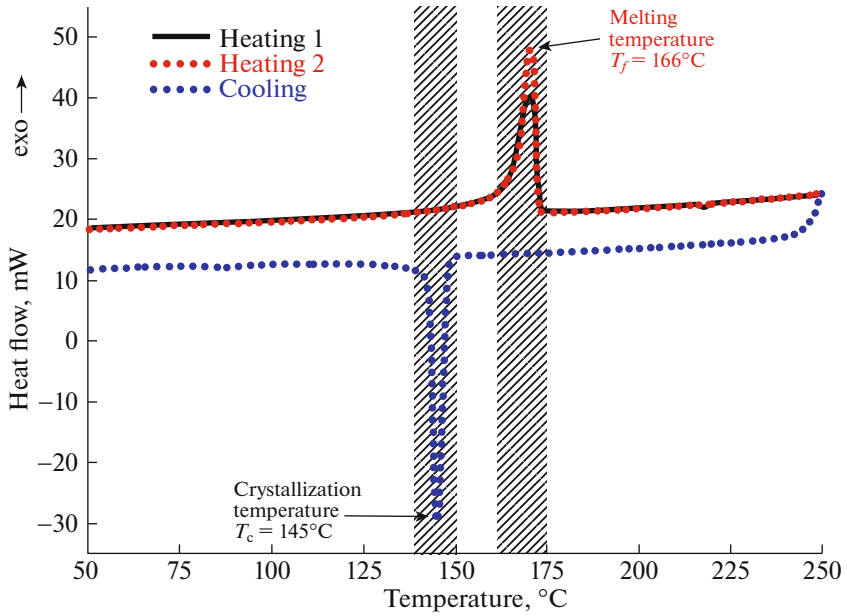

Fig. 11. DSC thermogram of polyoxymethylene (POM).

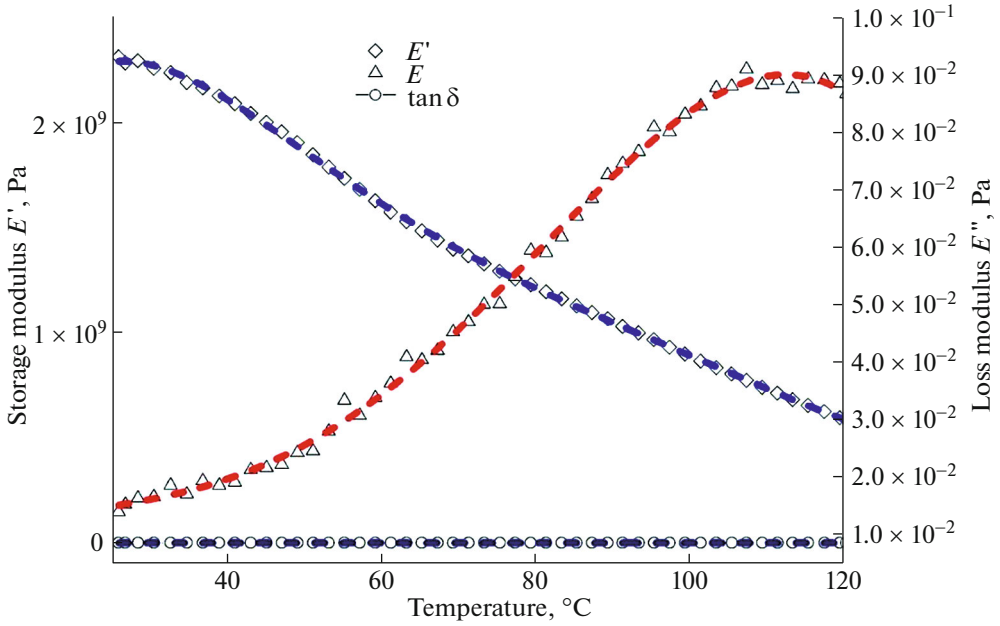

Fig. 12. The dependence of storage and loss modulus as a function of temperature of polyoxymethylene (POM).

porates damage mechanisms. This model should take into account phenomena such as void growth and coalescence, which are critical to understanding the material's performance under very large deformations. These mechanisms are essential for predicting failure in polymers, particularly under conditions of high stress and strain. The development of this plasticity model will enable more accurate predictions of material performance, guiding the design and selection of suitable substitutes for POM in various applications. This approach will not only enhance our understanding of the material's capabilities but also facilitate the development of new polymers with tailored properties to meet the stringent demands of modern engineering applications. In conclusion, while substituting POM remains a challenging endeavour, the comprehensive

analysis provided in this work lays a solid foundation for further research and development. By advancing our modelling capabilities and exploring innovative materials, we can move closer to finding viable alternatives that replicate the unique properties of POM.

ACKNOWLEDGMENTS

The authors extend their appreciation to Taif University, Saudi Arabia, for supporting this work through project number (TU-DSPP-2024-208).

AUTHOR CONTRIBUTION

Conceptualization: Sid Ahmed Reffas

Data curation: M. Elmmaguenni, R. Yekhlef, A. Djemli

Formal analysis: D. Belfennache

Methodology, validation: M. Fatmi, Talal M. Althagafi

FUNDING

This work was supported by ongoing institutional funding. No additional grants to carry out or direct this particular research were obtained.

DATA AVAILABILITY

Data underlying the results presented in this paper are not publicly available at this time but may be obtained from the corresponding author (fatmimessaud@yahoo.fr) upon reasonable request.

CONFLICT OF INTEREST

The authors of this work declare that they have no conflicts of interest.

REFERENCES

1. R. Hsissou, R. Seghiri, Z. Benzekri, M. Hilali, M. Rafik, and A. Elharfi, Compos. Struct. **262**, 113640 (2021). https://doi.org/10.1016/j.compstruct.2021.113640
2. V. Shanmugam, K. Babu, G. Kannan, R. A. Mensah, S. K. Samantaray, and O. Das, Polym. Degrad. Stab. **228**, 110902 (2024). https://doi.org/10.1016/j.polymdegradstab.2024.110902
3. K. U. Claussen, T. Scheibel, H. W. Schmidt, and R. Giesa, Macromol. Mater. Eng. **297** (10), 938 (2012). https://doi.org/10.1002/mame.201200032
4. A. A. Askadskii, L. M. Goleneva, E. S. Afanas'ev, and M. D. Petunova, Rev. J. Chem. **2**, 105 (2012). https://doi.org/10.1134/S207997801202001X
5. P. Le Duc, C. Haber, G. Bao, G., and D. Wirtz, Nature **399** (6736), 564 (1999). https://doi.org/10.1038/21148
6. A. C. Lua and J. Su, Polym Degrad. Stab. **91**, 144 (2006). https://doi.org/10.1016/j.polymdegradstab.2005.04.021
7. J. M. Morancho, J. M. Salla, X. Ramis, and A. Cadenato, Thermochim. Acta **419**, 181 (2004). https://doi.org/10.1016/j.tca.2004.02.011
8. V. Mamleev, S. Bourbigot, M. Le Bras, and J. Lefebvre, J. Therm. Anal. Calorim. **78**, 1009 (2004). https://doi.org/10.1007/s10973-004-0467-7
9. M. Kroon and M. B. Rubin, Eur. J. Mech. A: Solids **100**, 105004 (2023). https://doi.org/10.1016/j.euromechsol.2023.105004
10. H. Cruz, A. L. Pinto, J. C. Lima, L. C. Branco, and S. Gago, Mater. Lett.: X **6**, 100033 (2020). https://doi.org/10.1016/j.mlblux.2019.100033
11. B. Kost, M. Basko, S. Kazmierski, E. Zygadło-Monikowska, M. Słojewska, and P. Kubisa, Polym. Chem. **16** (5), 598 (2024). https://doi.org/10.1039/d4py01194e
12. O. Luzanin, D. Movrin, V. Stathopoulos, P. Pandis, T. Radusin, and V. Guduric, Rapid Prototyping J. **25** (8), 1398 (2019). https://doi.org/10.1108/RPJ-12-2018-0316
13. I. E. Uflyand, E. G. Drogan, V. E. Burlakova, K. A. Kydralieva, I. N. Shershneva, and G. I. Dzhardimalieva, Polym. Test. **74**, 178 (2019). https://doi.org/10.1016/j.polymertesting.2019.01.004
14. M. Hesami and A. Jalali-Arani, Macromol. Mater. Eng. **303** (3), 1700446 (2018). https://doi.org/10.1002/mame.201700446
15. B. Rimez, G. Van Assche, S. Bourbigot, and H. Rahier, Polym. Degrad. Stab. **130**, 245 (2016). https://doi.org/10.1016/j.polymdegradstab.2016.06.021
16. S. Mouffok and M. Kaci, J. Appl. Polym. Sci. **132** (13), 41722 (2015). https://doi.org/10.1002/app.41722
17. N. Sun, J. Yang, Q. Gu, and D. Shen, J. Appl. Polym. Sci. **77**, 2044 (2000). https://doi.org/10.1002/1097-4628(20000829)77:9<2044::AIDAPP21>3.0.CO;2-K
18. W. Döll, Optical interference measurements and fracture mechanics analysis of crack tip craze zones, in *Crazing in Polymers, Advances in Polymer Science*, Vols. 52/53 (Springer, Berlin, 2005), p. 105. https://doi.org/10.1007/BFb0024057
19. C. B. Bucknall and R. R. Smith, Polymer **6**, 437 (1965). https://doi.org/10.1016/0032-3861(65)90028-5
20. A. S. Argon and J. G. Hannoosh, Philos. Mag. (1798-1977) **36**, 1195 (1977). https://doi.org/10.1080/14786437708239789
21. E. Passaglia, J. Phys. Chem. Solids **48** (11), 1075 (1987). https://doi.org/10.1016/0022-3697(87)90119-3
22. A. M. Donald, E. J. Kramer, and R. P. Kambour, J. Mater. Sci. **17**, 1739 (1982). https://doi.org/10.1007/BF00540802
23. L. L. Berger, D. J. Buckley, E. J. Kramer, H. R. Brown, and R. A. Bubeck, J. Polym. Sci., Part B:Polym. Phys. **25**, 1679 (1987). https://doi.org/10.1002/polb.1987.090250810

24. M. G. A. Tijssen, E. Van der Giessen, and L. J. Sluysa, Int. J. Solid. Struct. **37**, 7307 (2000). https://doi.org/10.1016/S0020-7683(00)00200-6
25. C. B. Bucknall, Polymer **48**, 1030 (2007). https://doi.org/10.1016/j.polymer.2006.12.033
26. C. G'sell and A. Dahoun, Mater. Sci. Eng. **175**, 183 (1994). https://doi.org/10.1016/0921-5093(94)91058-8
27. M. Dettenmaier and H. H. Kausch, Colloid Polym. Sci. **259**, 937 (1981). https://doi.org/10.1007/BF01524816
28. W. Zhao, Y. Wang, X. Wang, and D. Wu, Ceram. Int. **42** (5), 6329 (2016). https://doi.org/10.1016/j.ceramint.2016.01.022
29. M. Fischer, C. Blanco, Y. Spoerer, M. Stommel, and I. Kuehnert, Polym. Test. **140**, 108626 (2024). https://doi.org/10.1016/j.polymertesting.2024.108626
30. B. Stoltz and M. Kroon, Eur. J. Mech. A: Solids **112**, 105625 (2025).
31. R. Hill, *The Mathematical Theory of Plasticity* (Clarendon Press, Oxford, 1950).